

Strain Hardening Behavior of Heat-Treated Austenitic Manganese

Stan Kristian G. Ejera¹, Lemuel N. Apusaga², and Manolo G. Mena¹

¹Department of Mining, Metallurgical and Materials Engineering, University of the Philippines-Diliman

²Materials and Process Research Division Metals Industry Research and Development Center

Corresponding author: sgejera@up.edu.ph

Abstract – Austenitic manganese steel (AMS), also known as Hadfield Steels, is a type of steel alloy known for its excellent toughness, ductility, wear resistance, and work-hardening capability. This study explores the strain-hardening behavior of AMS. The effects of both casting pouring temperature (1370, 1410 and 1450 °C) and microalloying (0.1% Ti and 0.06% Ce) were investigated. The samples were melted in an induction furnace, sand-cast at varying pouring temperatures, and then heat treated at 1090°C for 2 hours. The heat-treated samples were then subjected to tensile testing — raw data of which were used in mathematical analysis to find the strain hardening exponents (n_1 and n_2), instantaneous strain hardening exponent (n^*), and strain hardening rate ($d\sigma/d\epsilon$). Results show that coarser grain sizes resulted in higher n -values with sharp transitions from the plastic to the brittle state. Conversely, finer grain sizes resulted in smaller n -values with a gradual decline in their formability/plasticity as opposed to the sudden drop observed in courser grains. The introduction of alloying elements lowers the n -value due to their secondary strengthening effects (e.g. 2nd phase and solid solution strengthening) and may offset any positive grain size effect on the alloy's formability in the low to intermediate strain range. These secondary effects, however, are less prominent at advanced strain levels. Lastly, larger grain sizes and possibly secondary strengthening effects markedly increase the calculated strain hardening rate over the plastic region.

Keywords: Austenitic Manganese Steel; Hadfield Steel; Pouring Temperature; Strain Hardening

I. INTRODUCTION

Austenitic Manganese Steels (AMS), also known as Hadfield steels is a type of alloy steel used in high- impact and wear applications. Its high toughness, good ductility, and excellent work-hardenability are ideal for such applications [1]. When hard materials are exposed to high- impact and wear conditions, impact-induced brittle fracture commonly occurs. However, AMS retains its toughness over a wide range of strain hardening preventing such brittle fractures [2]. In the Philippines, mining and quarry companies mainly utilize AMS in crusher plates, grinding mill liners, cement mixers, impact hammers, transportation equipment, etc.

Sir Robert Hadfield, a metallurgist whom the alloy is named after, conducted several experiments on high manganese steels in 1882. His experiments found that 12% Mn and 1.2% C were the optimum composition to achieve the best properties. He also found that an Mn:C ratio of 10:1 is ideal. In today's manufacturing, AMS steels have a similar composition to that of Hadfield's original alloy with Mn ranging from 12% to 15%. Emerging manganese steels today, however, can have Mn content higher than 20% [1,3].

Austenite is a tough allotrope of iron with excellent mechanical properties and is only normally stable at high temperatures in unalloyed steels. The presence of Mn in Hadfield Steels allows austenite to be stable even at room temperature. This results in a predominantly austenitic microstructure — thus, is also why *austenitic manganese steel* is a term used interchangeably with *Hadfield steel*. The main difference between austenite and ferrite (the normal iron phase at room temperature for unalloyed steels) is their crystalline structure – face-centered cubic (FCC) for the former and body-centered cubic (BCC) for the latter. The friction stress of dislocations in FCC structures is far lower than in BCC giving austenite better plasticity, i.e., higher ductility. This allows the absorption of more energy without fracturing. The austenitic structure, together with the formation of dispersed hard carbides make AMS a superior alloy in the industry.

Since AMS is mostly used in applications where the metal experiences extreme stresses, it is important to understand its behavior in response to these stresses. For most metals, this response can be fully characterized by the strain hardening (or work hardening) effect wherein materials gain a significant increase in strength when undergoing plastic deformation. This study aims to explore these strain-hardening behaviors. Ultimately, the goal of the study is to help local industries understand the limitations as well as optimize the use of AMS in specific service conditions.

II. METHODOLOGY

2.1 Sand Casting Procedure

The samples were melted in an induction furnace and sand-cast at varying pouring temperatures. Manganese steel scraps were used as the starting base alloy for the furnace charge. To reach the target elemental composition, two alloy adjusters were used – ferromanganese alloy for Mn and carbon raisers for C. Mild steel scraps were added as needed for dilution. The target composition, based on the nominal specifications for Hadfield steels, is given in Table 1 [4].

Table 1. Composition, wt%

	Fe	Mn	C	Cr
Target	85.9	12.5	1.1	0.5
Actual	84.24	12.45	1.54	1.78

The initial charge was calculated based on the raw materials' chemical composition. After the melt had homogenized, a sample was collected and elementally analyzed using an Optical Emission Spectrometer (OES). Iterative adjustments using the alloy adjusters were done until the target composition was met. A comparison of the target and actual final composition is also shown in Table 1.

With the target composition met, the melt was ready for pouring. Three pouring temperatures, which were carefully measured through an immersion thermocouple at the ladle,

were used for the study. These were 1370, 1410 and 1450°C. Once the required pouring temperature had been reached, the molten metal inside the ladle was poured into the molds which were then air-cooled overnight. Figure 1 shows the schematic diagram of the casting setup. The castings had a 32 mm cross-sectional diameter and overall rectified length of roughly 1500 mm. These were cut into smaller pieces roughly 40 mm length, and used as samples for the different characterization and mechanical tests.

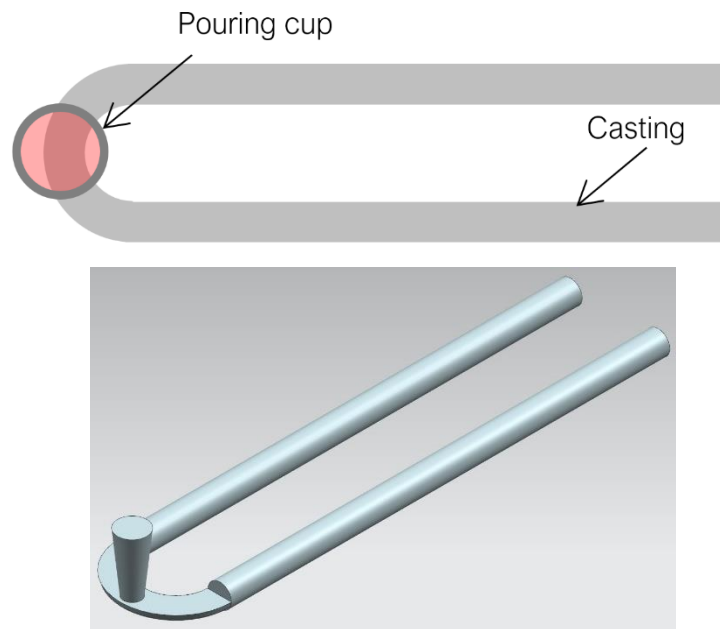


Figure 1. Schematic diagram and 3D render of casting.

2.2 Micro-alloying Procedure

Two common alloying elements for AMS, namely Ti and Ce, were chosen for this study following literature review. The alloying elements were added directly into the ladle just prior to the pouring stage. The appropriate amount (in grams) of Ti and Ce were pre-calculated to achieve a final concentration of 0.1% and 0.06%, respectively. The solid additives were allowed to melt and homogenize with the molten AMS in the ladle before the final pour.

2.3 Heat Treatment

Hadfield Steel is too brittle to be used as-cast. Heat treatment is usually done to improve its ductility and overall toughness. In this study, heat treatment was carried out at an elevated temperature of 1090°C for 2 hours using a muffle furnace. Samples were immediately quenched in water afterwards producing the final internal structure.

2.4 Mechanical Testing

Stress-strain data were obtained using a universal testing machine (UTM). Test coupons for the tensile test were acquired by cutting 100mm-long sections from the heat-treated specimens. To prevent any alteration of microstructure, the casting was sectioned using a

water-cooled abrasive cutter. These were then machined to dimensions specified by ASTM E8 as seen in Figure 2. The strain rate for the tensile test was set to 0.5 min^{-1} .



Figure 2. Images of (a) machined samples for tension test and (b) sample undergoing tension test

2.5 Grain Size Measurement

Cylindrical sections of 25 to 38 mm in length were cut from the heat-treated cast product for metallographic examination. The samples were ground using SiC paper at increasing grit sizes from 80p to 1200p. Polishing was done using suspended gamma alumina. Nital (2-5% v/v) was the etchant of choice to expose the necessary metallographic features.

The grain size was determined using Saltykov's Planimetric Method. In this method, test rectangles, instead of circles used in Jeffries' method, were overlaid onto the micrographs where the whole (inside) grains and half (intercepted) grains contained in the test rectangles were counted and used to determine the average grain size, d (in mm). This was done with the aid of a free and open-source software, ImageJ. An example can be seen in

Figure 3. The average grain size was computed using:

$$N_A = f(N_{inside} + N_{intercepted})$$

$$d = \sqrt{\frac{1}{N_A}} \quad (1)$$

where N_A is equal to the average number of grains per mm^2 , f is the reciprocal of the actual area of the test rectangle (in mm^2), N_{inside} is the number of whole grains inside the test rectangle, and $N_{intercepted}$ is the number of half grains intercepted at the perimeter of the test rectangle.

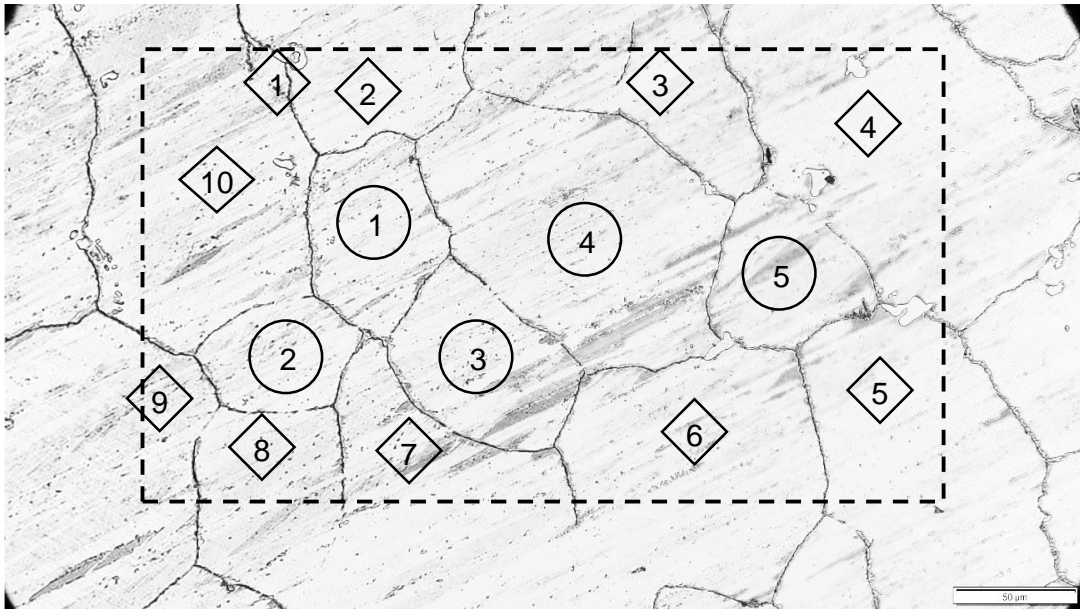


Figure 3. Saltykov’s Planimetric Method using ImageJ software. The test area is depicted by the broken rectangle. Encircled numbers indicate whole grain count while those inside triangles indicate half grain count.

2.6 Mathematical Analysis

The plastic region of a stress-strain diagram, which shall be the region of interest in this study, is the region from the yield point (using 0.2% offset yield stress) to the UTS point. This can be sufficiently described by the Hollomon equation:

$$\sigma = K\varepsilon^n \tag{2}$$

where σ is the true stress, ε is the true strain, and n is the strain hardening exponent (SHE). Oftentimes, the true strain in the Hollomon equation is just taken as the total strain (sum of elastic and plastic strains) since the elastic strain contribution is usually negligible. However, for cases where the elastic contribution is significant (as is the case in this study which will be discussed further in section III.1.), the use of true plastic strain is more appropriate. This can be calculated through:

$$\begin{aligned} \varepsilon_t &= \varepsilon_p + \varepsilon_e \\ \varepsilon_t &= \ln(1 + e) \\ E &= \frac{\sigma}{\varepsilon_e} \\ \sigma &= s(1 + e) \\ \varepsilon_p &= \ln(1 + e) - \frac{s(1 + e)}{E} \end{aligned} \tag{3}$$

where the subscripts p , t and e correspond to *plastic*, *total* and *elastic* strains, respectively. The *Latin* variables s and e represent the *engineering* stress and strain values, respectively; while

the *Greek* variables σ and ε are the *true* stress and strain values. Lastly, the constant E is the modulus of elasticity which can be derived from the *engineering* stress-strain (s - e) curve by taking the slope of the linear region (from $e = 0$ to $e =$ yield strain – where yield strain is the strain corresponding to the 0.2% offset yield stress).

Taking the natural logarithm of both sides of the Hollomon equation (2), yields

$$\ln(\sigma) = \ln(K) + n \times \ln(\varepsilon) \quad (4)$$

which is a linear equation with slope equal to n . Thus, if a double logarithm plot (using $\ln(\sigma)$ in the y-axis and $\ln(\varepsilon)$ in the x-axis) of a *true* stress-strain diagram were constructed within the region of interest a resulting straight line should be produced where the n -value, SHE, can be derived.

Yet another way to calculate SHE is by computing for the instantaneous value as straining progresses. This becomes extremely useful when the metal does not display a distinct *single-n* behavior and/or if the SHE behavior/trend is more important than the overall n -value itself. This can be done by taking two (σ, ε) test points and substituting them to eq. (4). This gives a system of two (2) equations where n can be calculated:

$$\begin{aligned} \ln \sigma_1 &= \ln K + n^*(\ln \varepsilon_1) \\ \ln \sigma_2 &= \ln K + n^*(\ln \varepsilon_2) \\ \ln \sigma_2 - \ln \sigma_1 &= \ln K - \ln K + n^*(\ln \varepsilon_2 - \ln \varepsilon_1) \\ n^* &= \frac{\Delta \ln \sigma}{\Delta \ln \varepsilon} \\ n^* &= \frac{\ln \left(\frac{\sigma_2}{\sigma_1} \right)}{\ln \left(\frac{\varepsilon_2}{\varepsilon_1} \right)} \end{aligned}$$

or

$$n^* = \frac{\ln (\sigma_{i+m}/\sigma_{i-m})}{\ln (\varepsilon_{i+m}/\varepsilon_{i-m})} \quad (5)$$

where $(\sigma_{i-m}, \varepsilon_{i-m})$ and $(\sigma_{i+m}, \varepsilon_{i+m})$ are the two test points. The subscript i represents the instantaneous/central point while m is the chosen distance (no. of data points) away from i . To differentiate this instantaneous SHE from the previously calculated n -value, this shall be referred to as n^* .

Lastly, the instantaneous strain hardening rate, $\frac{d\sigma}{d\varepsilon}$, at any point in the region of interest can be calculated by taking the slope of the tangent line at that specific point in a stress-strain plot. This can be approximated by taking the *rise-over-run* of test points surrounding the vicinity of a point of interest $(\sigma_i, \varepsilon_i)$.

$$\frac{d\sigma}{d\varepsilon} \approx \frac{\Delta\sigma}{\Delta\varepsilon} = \frac{\sigma_2 - \sigma_1}{\varepsilon_2 - \varepsilon_1} = \frac{\sigma_{i+m} - \sigma_{i-m}}{\varepsilon_{i+m} - \varepsilon_{i-m}} \quad (6)$$

As with the n^* calculation, m here is again a chosen distance (no. of data points) away from the central point of interest i .

III. RESULTS AND DISCUSSION

3.1 Effect of Pouring Temperature

Before doing any strain hardening analysis, it is of paramount importance to establish whether true strain in eq. (2) be expressed in terms of total strain or plastic strain. A graph of the elastic strain contribution vs. the total strain seen in Figure 4 shows that the elastic contribution is quite significant. Matusevich et al. [5] suggest, as per ASTM 646 standard, that plastic strain should be used in place of total strain when elastic strain contribution is greater than 10%. In the figure, the elastic contribution for all samples never goes below 30% in the region of interest. This is also true for the micro-alloyed samples that will be discussed in the succeeding subsection. Therefore, plastic strain ϵ_p , as defined in eq. (3), will be used for equations (4), (5), and (6).

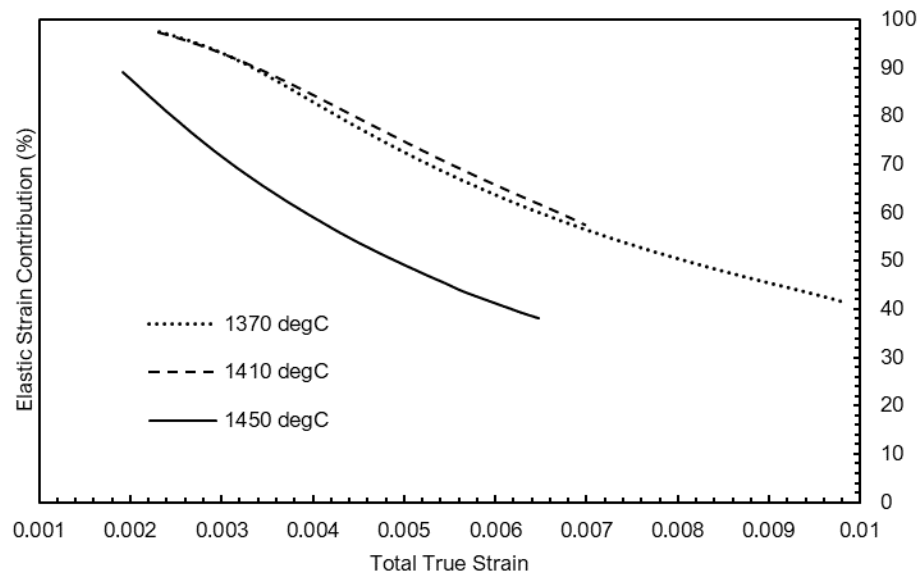


Figure 4. Elastic strain contribution vs. total true strain

The true stress-strain diagram of the unalloyed samples is seen in Figure 5. As discussed in subsection II.6., we can derive SHE by converting the x- and y- axes into logarithmic scale thus producing a double logarithm plot.

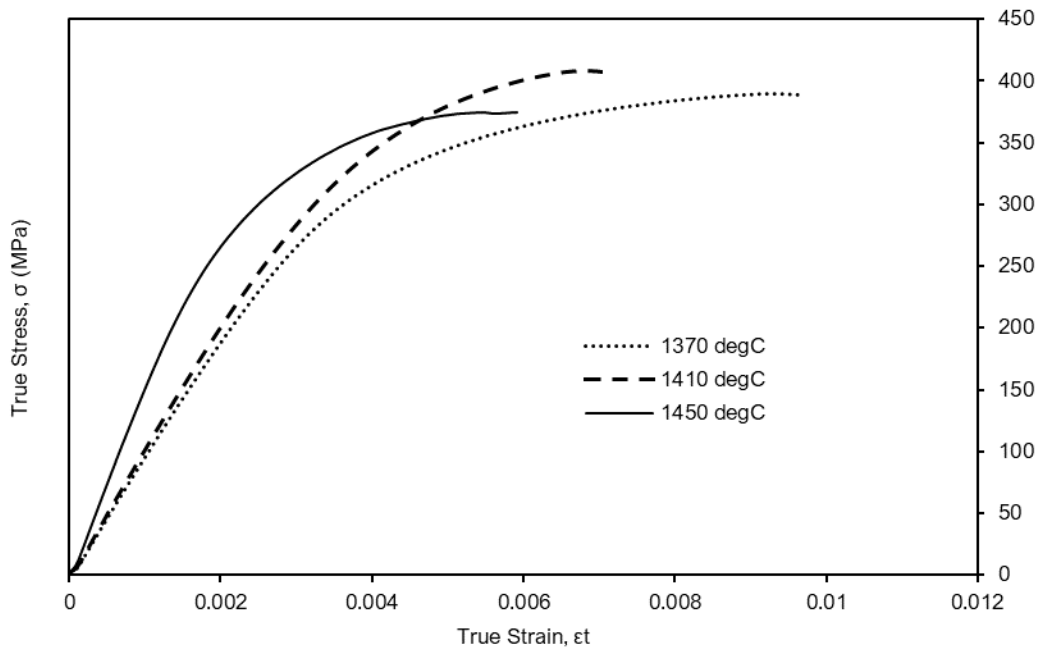


Figure 5. True stress-strain diagram of unalloyed AMS poured at different temps. Data is trimmed at UTS.

The resulting double logarithm plot for the unalloyed AMS is shown in Figure 6. It is interesting to note that all three samples exhibit what is known as a *double- n behavior* wherein two n -values can be derived by establishing an inflection point. This is a well-known phenomenon reported in steel alloys [6].

As seen in Figure 6 and summarized in Table 2, the n_1 values for the two lower temperatures are quite similar. This indicates that at low to intermediate strains the strain hardening behavior for AMS poured at 1370 and 1410 °C are quite similar. The high pouring temperature shows a smaller n_1 value. Moreover, the n_2 values show the same pattern — higher and similar values for the two lower pouring temperatures and a noticeably smaller value for the highest pouring temperature.

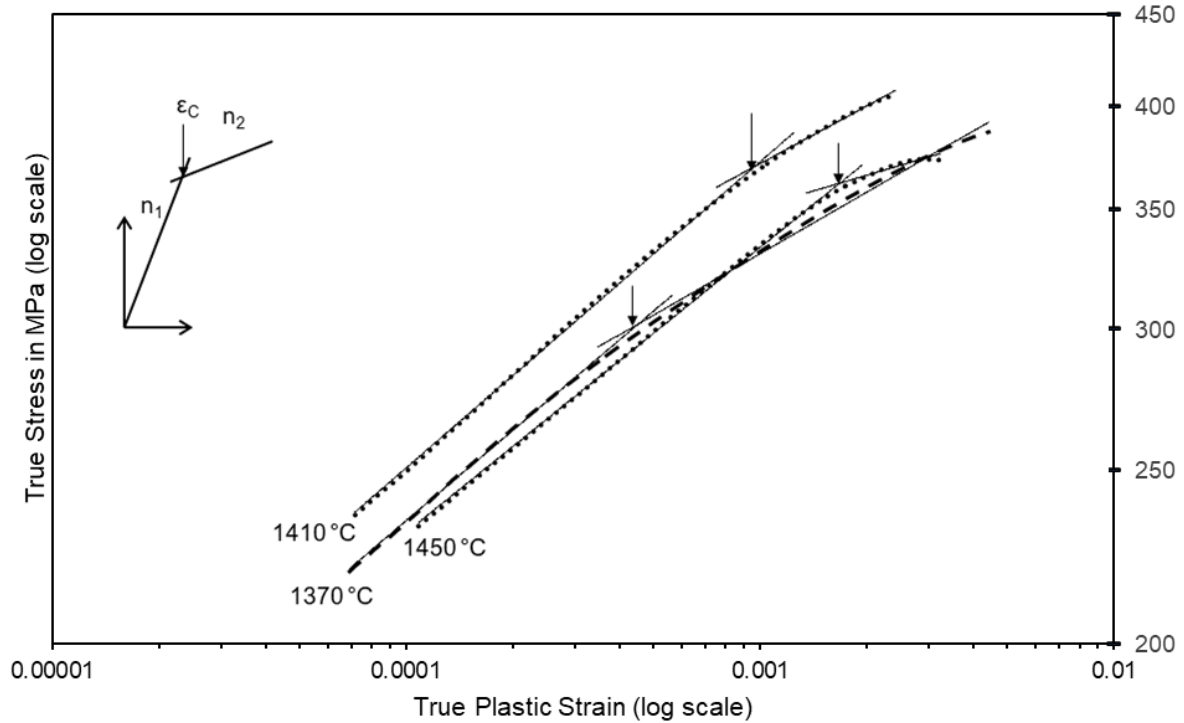


Figure 6. Log-log plot of stress-strain diagrams for unalloyed AMS poured at varying temperatures showing good linearity.

Table 2. Summary of strain hardening data for unalloyed AMS at varying pouring temp.

Pouring Temp., °C	Grain Size, microns	n_1	n_2	ϵ_c
1370	443	0.1681	0.1143	0.00046
1410	408	0.1716	0.1072	0.00098
1450	363	0.1599	0.0584	0.00171

The SHE is, essentially, a measure of the formability of a metal. A higher value translates to a better ability to strain harden further with increasing plastic deformation. As metals strain harden, their capacity for further work hardening decreases resulting in a lower SHE value.

From the previous study done by the authors, it was found that lowering the pouring temperature during the casting stage, increases the final grain size after heat treatment. This is due to the difference in availability of free energy related to thermal straining prior to heat treatment. Bearing this in mind, it can be deduced that larger grain sizes equate to higher n values as well. This is in good agreement with other work hardening studies done [6,7].

At larger grain sizes, there are fewer hindrances to dislocation motion and nucleation. Thus, the material can undergo more plastic deformation which leads to further strain-hardening. That is to say, because grain size is large, onset flow stress (yield stress) is smaller providing for a higher “ceiling” for which strengthening via strain hardening can occur. Conversely, at

finer grain sizes, dislocation forests/entanglement is readily attained thus the capacity to further strain harden is limited. This is why the n_2 values are significantly smaller than n_1 . At these advanced strain ranges, the material is already at an extremely strain-hardened state resulting to reduced formability. This grain boundary explanation is further evidenced by the strain hardening plot shown in Figure 7. The lower pouring temperatures (1370°C and 1410°C; which have higher grain sizes) show higher strain hardening rates compared to the 1450 °C sample (smaller grain size). This is true for every stage in the region of interest. Higher strain hardening rates illustrate the rapid increase in flow stress with increasing plastic deformation and should be indicative of the material's formability, or capacity to be work-hardened.

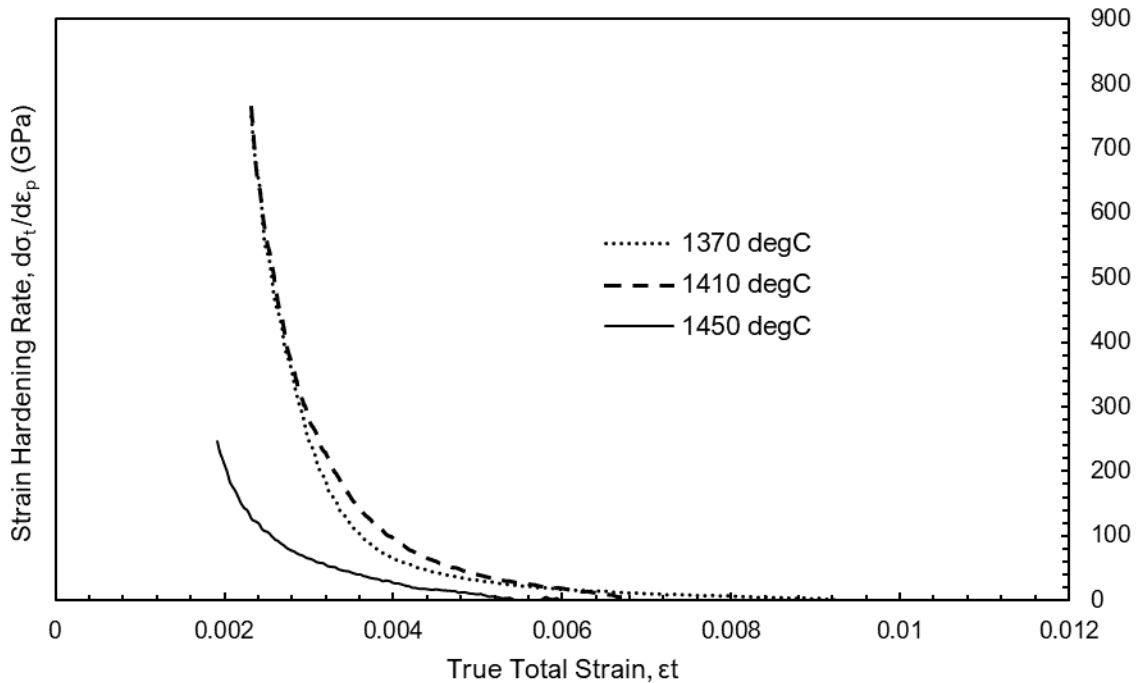


Figure 7. Strain hardening rate vs. total strain of AMS poured at varying temperatures.

One interesting feature of plots with *double-n behavior* is the strain point, ε_c — which is the intersection between the two straight trendlines whose slopes are n_1 and n_2 . Miyakusu et al. [6] used the same technique in determining ε_c in their study on the strain hardening of ferritic steels. This value roughly corresponds to the inflection point discussed earlier. The ε_c indicates that there exists a threshold beyond which the strain hardening behavior drastically changes from a “formable” (high n_1) to a “non-formable” (low n_2) state. It can be observed that there is an increasing ε_c trend with decreasing grain size. This might mean that at smaller grain sizes, it takes advanced strain levels to change its formable state while at larger grain sizes, the threshold is reached much earlier. Although this is a useful observation, the instantaneous SHE (n^*) seen in eq. (5) should be able to better describe and confirm this transition trend from the “formable” to the “non-formable” state.

By plotting n^* with the true plastic strain, the alloy's formability trend can be tracked as it is being plastically deformed as seen in Figure 8. It is noticeable that at the n_1 ranges, the plots

are relatively flat which is an indication of consistent strain-hardening behavior. At further strains, however, the n^* drops eventually. The trends indicate that higher pouring temperature (lower grain sizes) translates to sharper and more drastic drops in n^* as strain progresses. Conversely, at the lower temperatures (higher grain sizes), it can be observed that the transition is more of a steady decline over a wide strain range rather than a sharp drop. This implies that coarse-grained AMS will likely experience a slow and steady shift from a plastic behavior to a brittle one over a wider range of plastic deformation. While in fine-grained AMS, plastic behavior will be more consistent but rapidly changes to a brittle behavior at advanced strain levels. Lastly, it is quite interesting that the ϵ_c corresponds quite well with where the curves fall off, whether sharp or slow. This is a good indicator of the robustness of the mathematical analysis used.

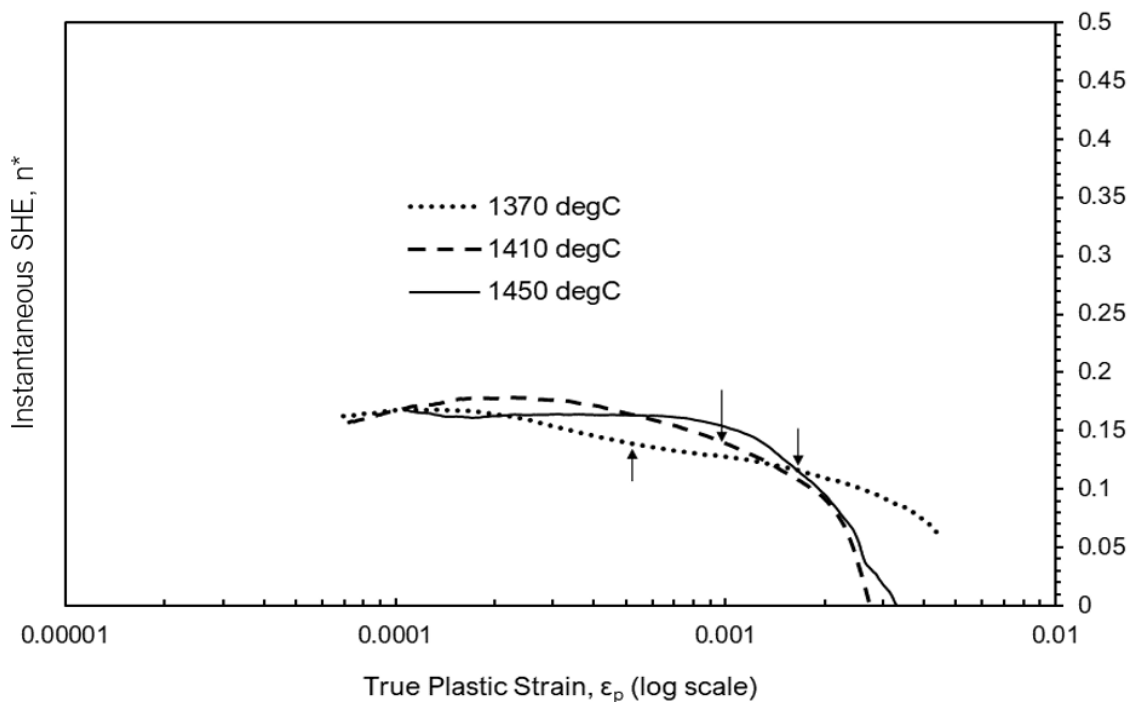


Figure 8. Instantaneous strain hardening exponent, n^* vs. the true plastic strain of unalloyed AMS at varying pouring temperatures. Arrows indicate where ϵ_c is located.

3.2 Effect of Alloying Elements

Despite having negative effects on the stiffness of the AMS, both alloying elements produced marked increases in strength. The Ti-alloyed AMS has the highest strength but also, however, produced the narrowest plastic region making it the most brittle of the three. Cerium, on the other hand, is an exceptional alloying element increasing both strength and ductility of the AMS producing not only a strong but also tough material. These initial observations can be seen in the true stress-strain diagram in Figure 9.

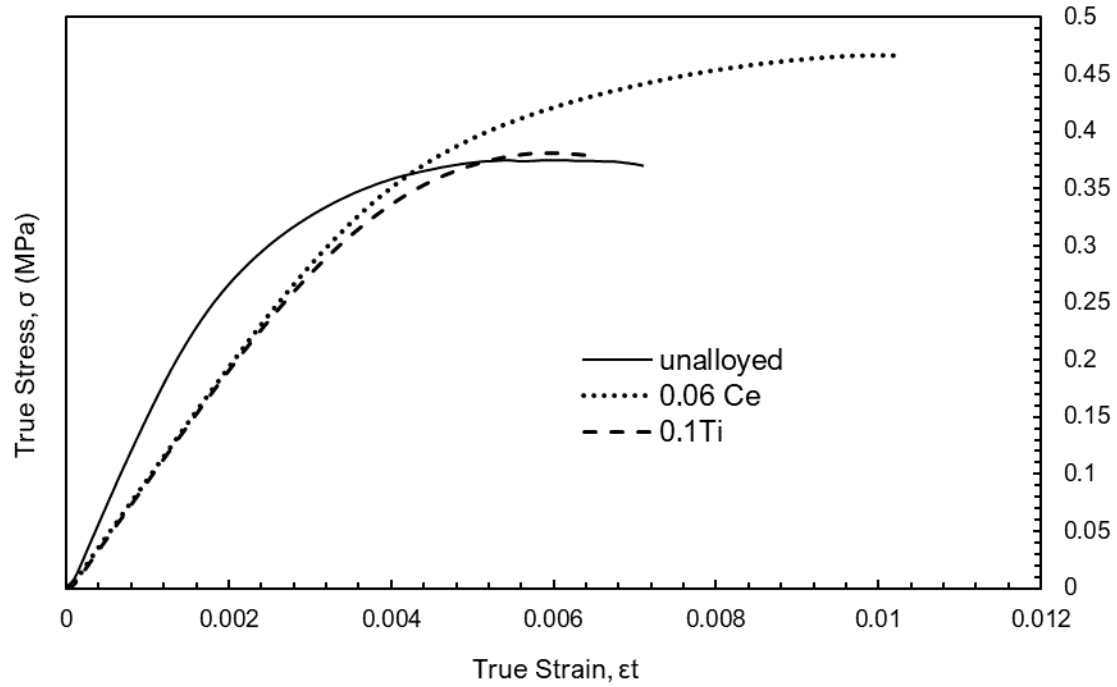


Figure 9. True stress-strain diagram of unalloyed vs. micro-alloyed AMS. Data is trimmed at UTS.

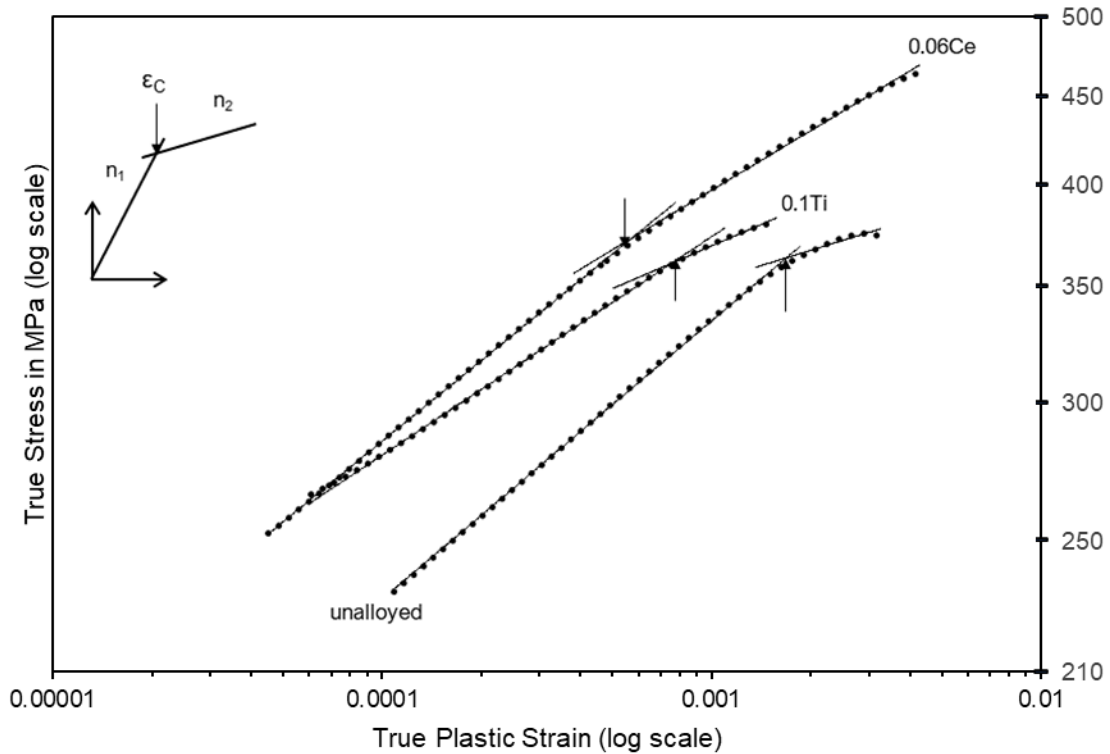


Figure 10. Log-log plot of stress-strain diagrams for unalloyed AMS vs. micro-alloyed AMS showing good linearity.

Table 3. Summary of strain hardening data for unalloyed AMS vs. micro-alloyed AMS.

Alloying, wt%	Grain Size, microns	n_1	n_2	ϵ_c
0.06 Ce	984.43	0.1541	0.1139	0.00057
0.1 Ti	458.38	0.1256	0.0817	0.00076
none	363	0.1599	0.0584	0.00171

Data from Table 3 which is extracted from Figure 10 shows some contradictions to the trends seen in the previous subsection III.1. Firstly, the Ti-alloyed AMS, despite having the larger grain size, produced a smaller n_1 value compared to the unalloyed AMS. The same thing can be said for the Ce-alloyed AMS which is almost three times larger in grain size compared to the unalloyed AMS but did not translate to a high n_1 value as expected.

This contradiction could be explained by the other dislocation-hindering mechanisms these alloying elements introduce. Titanium, on one hand, is known to produce nitrides and carbides (2nd phase precipitates) in AMS. The previous study the authors have conducted confirms this. Second phases are excellent hindrances to dislocation motion which should contribute significantly to the limiting of the capacity to work-harden and thus lowering the n_1 value. Silva, et al. [8] also noted this phenomenon in their work on steel pipes. Meanwhile, Ce has been shown in the previous study to exhibit solid solution strengthening. Solid solutions, like 2nd phases, also impede dislocation motion by straining the lattice. This is to say that the supposed positive increase in n_1 brought about by the very large grain size of the 0.06Ce AMS is completely offset by the negative decrease in formability brought about by the solid solution effect.

The n_2 values, however, follow the previously established trend in subsection III.1. This might imply that the secondary strengthening mechanisms of Ti and Ce (2nd phase and solid solution, respectively) are significant only in the low to intermediate strain ranges. At more advanced strain levels, dislocation pileup at grain boundaries may be the predominant strain hardening mechanism making the secondary strengthening influence less pronounced, if not non-existent. This is further supported by the 0.06Ce sample where because of its extremely coarse grains, dislocation pileup is not readily available even at further strain ranges despite the solid solution lattice strains. This makes it such that the n_2 value does not drop off as observed in the other cases but, on the contrary, remains almost equal to the n_1 value. This leads to the Ce-alloyed AMS exhibiting an almost *single-n behavior*.

Even though the micro-alloyed AMS had lower n -values (which should mean lower strain hardening rates), the grain boundary effect on the strain hardening rate observed in subsection III.1 is still quite apparent when looking at the graphs in Figure 11. Here we can see that the micro-alloyed AMS (which have the larger grain sizes by a good margin) have markedly higher strain hardening rates when compared to the unalloyed counterpart (lower grain size). In fact, in the low to intermediate strain range, the difference is quite stark. That said, it seems that strain hardening rates are much more related to the grain size rather than the formability (n value), per se. It could also be possible that the secondary strengthening effects, despite

lowering formability, also increase the strain hardening rate. There might be more complex interactions at play which requires further investigation.

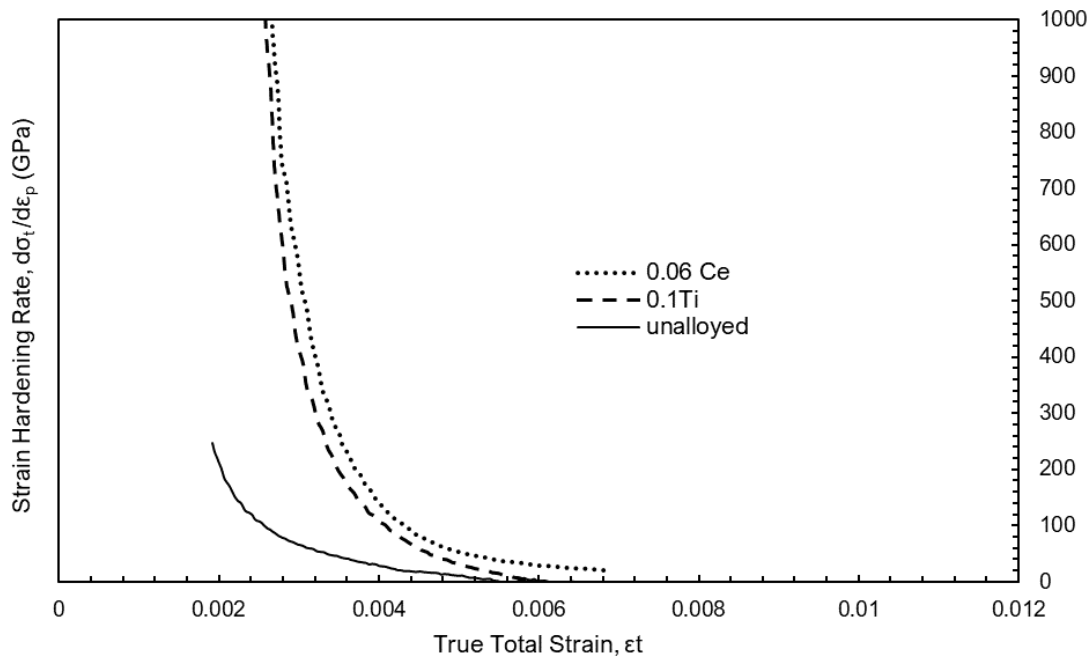


Figure 11. Strain hardening rate vs. total strain of unalloyed and micro-alloyed AMS.

Lastly, the n^* comparisons in Figure 12 yield interesting outcomes. Again, for the unalloyed AMS, the trend is familiar – a relatively flat curve at the n_1 range followed by a sharp drop corresponding to the ϵ_c value. The Ti-alloyed AMS is unique as it has an almost *hill curve* with an n^*_{max} value equal to the computed n_1 value. This indicates that the formability of the 0.1Ti AMS is not at all consistent. It also has the observed sharp drop off at ϵ_c . Moreover, it has the lowest n^* value at any point in the region of interest which alludes to the fact that it was initially shown to be very brittle because of its short plastic region. Again, a low n -value is indicative of a brittle material with low formability/plasticity. The Ce sample has lower n -values than that of the unalloyed one but it is more consistent over a wide range of strain. Its plot shows little drop off and remains relatively flat. This indicates that although it has lower formability, its strain-hardening behavior is consistent and shows no sudden brittle transformation. The flatness of its n^* curve also agrees with its nearly *single-n behavior* mentioned earlier in the discussion.

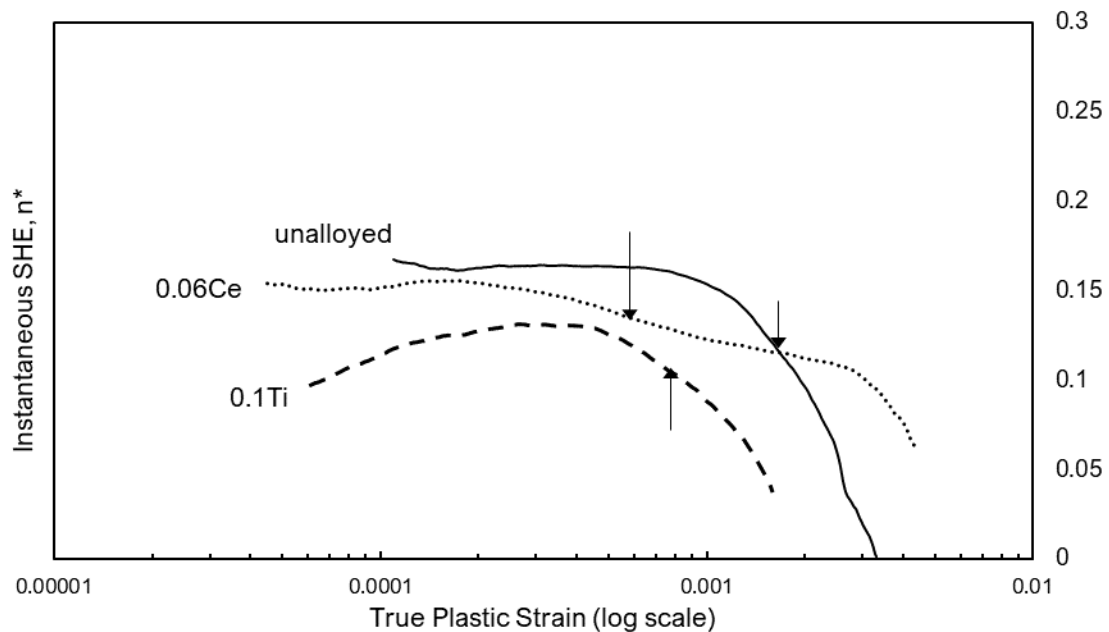


Figure 12. Instantaneous strain hardening exponent, n^* vs. the true plastic strain of unalloyed vs micro-alloyed AMS. Arrows indicate where ϵ_c is located.

IV. CONCLUSIONS AND RECOMMENDATIONS

Based on the results and discussion, the following conclusions can be made:

1. Almost all samples experience a double- n behavior to varying extents. The first n -value, n_1 , is larger corresponding to the specimen's "formable" state while the second n_2 value is smaller corresponding to its "non-formable" state. This behavior is expected as strain hardening causes metals to transform from an initial ductile to a more brittle final state. Only the Ce-alloyed specimen showed a possible single n -behavior.
2. The instantaneous SHE, n^* is a good measure of the changes in formability of the specimen as straining progresses. Two distinct behaviors are observed -- a steady slow decline versus a sharp drop at a particular inflection point.
3. For unalloyed AMS, larger grain sizes equate to higher n values due to fewer hindrances to dislocation motion and nucleation.
4. The micro-alloyed specimens, however, despite having larger grain sizes did not show equivalently higher n -values. This may be due to the other dislocation-hindering mechanisms brought about by the alloying elements. Titanium, on one hand, is known to produce nitrides and carbides (2nd phase precipitates) in AMS. Meanwhile, Ce has been shown to exhibit solid solution strengthening.
5. For all samples, it was observed that the larger grain sizes display higher strain hardening rates, $\frac{d\sigma}{d\epsilon}$. Strain hardening rate is indicative of a material's formability, or

capacity to be work-hardened. For larger grain boundaries, the "ceiling" for strain-hardening to occur is higher.

Despite the significant findings, it is recommended that future research do replicated runs when exploring this type of analysis. Outliers or gross errors might be hard to detect for unreplicated runs – such is the case with this study.

References:

- [1] Pathak S, Maharshi A. 2015. Development of a new etchant for austenitic manganese steel. *Journal of Advanced Research in Manufacturing, Material Science & Metallurgical Engineering*. 2(1).
- [2] Okechukwu C, Dahunsi O, Oke P, Oladele I, Dauda M. 2017. Prominence of hadfield steel in mining and minerals industries: A Review. *International Journal of Engineering*. 3(2):83-90.
- [3] Mahlami C, Pan X. 2014. An overview on high manganese steel casting. *Advanced Sustainable Foundry*. 1(1):420-428.
- [4] Subramanyam DK, Swansiger AE, Avery HS. 1990. *ASM metals handbook*. 10th ed. American Society of Metals International. p. 822–840.
- [5] Matusевич AE, Massa JC, Mancini RA. 2012. Computation of tensile strain-hardening exponents through the power-law relationship. *Journal of Testing and Evaluation*. 40(4).
- [6] Miyakusu K, Uematsu Y, Hoshino K. 1986. Effect of alloying elements on strain hardening exponent of ferritic stainless steel. *Transactions of the Iron and Steel Institute of Japan*. 26(3):228–235.
- [7] Antoine P, Vandeputte S, Vogt JB. 2005. Effect of microstructure on strain-hardening behaviour of a Ti-IF steel grade. *Iron and Steel Institute of Japan International*. 45(3):399–404.
- [8] Silva R, Pinto A, Kuznetsov A, Bott I. 2018. Precipitation and grain size effects on the tensile strain-hardening exponents of an API X80 steel pipe after high-frequency hot-induction bending. *Metals (Basel)*. 8(3):168.